



Cite this: *Phys. Chem. Chem. Phys.*,  
2021, **23**, 24052

# Desorption-induced evolution of cubic and hexagonal ices in an ultrahigh vacuum and cryogenic temperatures†

Gaurav Vishwakarma, Jyotirmoy Ghosh and Thalappil Pradeep \*

Reflection absorption infrared spectroscopic investigations of multilayer films of acetonitrile (ACN) and water in an ultrahigh vacuum under isothermal conditions showed the emergence of cubic (ice  $I_c$ ) and hexagonal (ice  $I_h$ ) ices depending on the composition of the film. The experiments were conducted with a mixed film of 300 monolayers in thickness and the ACN:H<sub>2</sub>O monolayer ratios were varied from 1:5 to 5:1. Mixed films were deposited at 10 K and warmed to 130–135 K, where ACN desorbed subsequently and IR spectral evolution was monitored continuously. While the emergence of ice  $I_c$  at 130 K has been reported, the occurrence of ice  $I_h$  at this temperature was seen for the first time. Detailed investigations showed that ice  $I_h$  can form at 125 K as well. Crystallization kinetics and activation energy ( $E_a$ ) for the emergence of ice  $I_h$  were evaluated using the Avrami equation.

Received 24th August 2021,  
Accepted 5th October 2021

DOI: 10.1039/d1cp03872a

rs.c.li/pccp

## 1 Introduction

The existence of water in diverse environments, as exotic as in space, is well known.<sup>1–3</sup> Water ice is known to exist in a number of amorphous as well as crystalline forms at different temperature and pressure conditions.<sup>4–7</sup> While ice  $I_h$  is the most dominant form in terrestrial conditions, it is known to exist above 150 K under an ultrahigh vacuum (UHV). The process of amorphous to crystalline transformation under UHV occurs generally by annealing the vapour deposited film, amorphous solid water (ASW), which involves multiple steps. At first, ASW is converted to ice  $I_c$  at temperatures between 100 and 150 K. This cubic form of ice is metastable in nature and is finally converted to the more stable ice  $I_h$  at temperatures higher than 150 K under an UHV,<sup>8</sup> a condition relevant to astrochemistry. However, ice  $I_c$  is, nowadays, termed as stacking-disordered ice (ice  $I_{sd}$ ) as its structure contains cubic sequences interlaced with hexagonal sequences.<sup>9,10</sup>

Impurities/guest molecules lead to diverse phenomena in the host ice network ranging from hydrate formation<sup>11–13</sup> to varying phase behavior.<sup>14,15</sup> They also play a crucial role in the crystallization of water. For example, crystallization kinetics of H<sub>2</sub>O can be enhanced by the addition of impurities like methanol, HCl and HNO<sub>3</sub>. Different reasons have been

suggested to explain these observations. While methanol-induced nucleation reduced the crystallization temperature,<sup>16</sup> excess proton (H<sup>+</sup>) provided by HCl promoted the crystallization.<sup>17</sup> Minor amounts of HNO<sub>3</sub> also facilitated rapid crystallization.<sup>18</sup> Under high-pressure conditions, however, clathrate hydrates can be transformed to ice  $I_c$  upon their dissociation.<sup>19–22</sup> Mixed ices can be warmed to form gas hydrates in an UHV; our earlier studies showed that clathrate hydrates of acetone and formaldehyde formed by such methods were converted to ice  $I_c$  and ice  $I_h$ , respectively, in the range of 130–135 K.<sup>12,23</sup> In such conditions, however, the formation of both ice  $I_c$  and ice  $I_h$  was not shown from a single system. Crystallization of H<sub>2</sub>O can also be achieved by several other methods such as annealing of amorphous ices,<sup>24,25</sup> supercooling of water droplets,<sup>26–29</sup> freezing of high-pressure ice phases followed by annealing<sup>25,30–32</sup> and freezing of water in confined geometries.<sup>33–35</sup> Hama *et al.*<sup>36</sup> showed that sublimation of a water/neon matrix leads to H<sub>2</sub>O crystallization where sublimation of neon provided enough mobility to water molecules to cross the kinetic barrier of crystallization, even at 11–12 K. These studies suggest the rich diversity that is possible during the desorption of molecules from multicomponent ices.

ACN was detected in the molecular clouds Sgr B and Sgr A<sup>37</sup> and in comet Kohoutek.<sup>38</sup> Comets are condensed bodies of gas, ice and dust, and are known for their diversity in composition with H<sub>2</sub>O as the most abundant species. But, in recent reports,<sup>39–41</sup> it was observed that comets C/2016 R2 (Pan-STARRS) and 2I/Borisov have a peculiar volatile composition with CO as the most abundant species. Volatiles are known to play a crucial role in the chemistry and physics of star

DST Unit of Nanoscience (DST UNS) and Thematic Unit of Excellence (TUE),  
Department of Chemistry, Indian Institute of Technology Madras, Chennai 600036,  
India. E-mail: pradeep@iitm.ac.in

† Electronic supplementary information (ESI) available: Isothermal time-dependent RAIR spectra, different crystallization parameters of H<sub>2</sub>O, and TPD-MS spectra of ACN in different mixtures. See DOI: 10.1039/d1cp03872a

formation in such regions. The present work hints at the importance of the composition of volatiles on water-ice crystallization and thus may have a direct impact on catalysis,<sup>8</sup> cometary outbursts, and heat balance in the cometary bodies.<sup>42</sup> These phenomena can be modeled with the help of experiments conducted in an UHV under cryogenic conditions.

In the present study, we show that ice  $I_c$  and ice  $I_h$  can be formed selectively from mixed ices of ACN and  $H_2O$  by controlling their compositions. We found that a thin film with 1:5 ACN and  $H_2O$  mixture forms ice  $I_c$  while a thin film with 5:1 ACN and  $H_2O$  results in ice  $I_h$  after desorption of ACN from the ice film at 130–135 K. The existence of the two ice forms has been confirmed by using their unique IR spectral features. The rates of crystallization of the films were studied using the Avrami equation. The activation energy for the formation of ice  $I_h$  under this condition was slightly lower than the value reported earlier. The creation of different crystallographic forms of ices by composition control presents new possibilities for structural diversity in interstellar ice analogues.

## 2 Experimental section

### 2.1 Experimental setup

All the experiments were performed in an ultrahigh vacuum (UHV) chamber with a base pressure of  $\sim 5 \times 10^{-10}$  mbar, discussed in detail elsewhere.<sup>43</sup> Briefly, the instrument is composed of three stainless steel UHV chambers: an ionization chamber, an octupole chamber, and a scattering chamber, used for low energy ion scattering of mass selected ions.<sup>44–47</sup> The instrument is equipped with reflection absorption infrared spectroscopy (RAIRS) and temperature-programmed desorption (TPD) mass spectrometry. Experiments were performed in the scattering chamber, fitted with a precision  $x$ - $y$ - $z$ - $\theta$  sample manipulator on which a closed-cycle helium cryostat (Coldedge Technologies) was mounted from the top, along with various probes focusing on the substrate. These vacuum chambers were pumped using a turbomolecular pumps, which were backed by several diaphragm pumps. A cold cathode gauge controlled using a MaxiGauge controller (Pfeiffer, Model TPG 256 A) monitored the vacuum in these chambers.

A highly polished Ru(0001) single crystal was used as substrate. The substrate was attached to a copper holder which in turn was connected at the tip of a closed-cycle helium cryostat (Zephyr HC-4A air-cooled compressor). The substrate temperature could be varied in a wide range of 8–1000 K with a temperature accuracy/uncertainty of 0.5 K. Different temperature sensors (K-type thermocouple and a platinum sensor) and a resistive heater (25  $\Omega$ ) were connected to a temperature controller (Lakeshore, Model 336).

### 2.2 Sample preparation

Before preparing the sample, the metal substrate was heated to 400 K multiple times to ensure the cleanness of the surface. The substrate was polished and annealed at 1000 K prior to the present set of experiments. As the experiments were of

multilayers and the results were insensitive to the impurities on the very top of the surface, detailed cleaning procedures were not necessary. ACN (RANKEM, 99.9%) and Millipore water ( $H_2O$  of 18.2 M $\Omega$  resistivity) were taken in a vacuum-sealed test tube (glass-to-metal seal) and further purified by several freeze-pump-thaw cycles. The samples were vapour-deposited on Ru(0001) using high-precision all-metal leak valves, one each exclusively for ACN and  $H_2O$ . The sample lines were kept near to the substrate for uniform growth of the thin ice films. During vapour deposition, mass spectra were recorded simultaneously to verify the purity, and to measure the ratio of the ACN and water vapours. Preparation of ice thin film was controlled through a leak valve and the coverage is expressed in monolayers (MLs), assuming  $1.33 \times 10^{-6}$  mbar s = 1 ML, which was estimated to contain  $\sim 1.1 \times 10^{15}$  molecules  $cm^{-2}$ , as outlined in several reports.<sup>11,48,49</sup>

### 2.3 Experimental procedure

Thin films of 300 MLs of ACN and  $H_2O$  were created by backfilling the vacuum chamber at a total pressure of  $\sim 5 \times 10^{-7}$  mbar for 10 minutes. Different ratios of ACN and  $H_2O$  (1:1, 1:5, and 5:1) were prepared at 10 K by keeping the total pressure constant and varying the inlet pressure of ACN and  $H_2O$  accordingly. For example, for the co-deposition (referred to as ACN: $H_2O$ ) of ACN and  $H_2O$  at a 1:1 ratio, the inlet pressure of ACN was  $\sim 2.5 \times 10^{-7}$  mbar and that of  $H_2O$  was  $\sim 2.5 \times 10^{-7}$  mbar. For the other ratios, the inlet pressures of ACN and  $H_2O$  were varied accordingly. Here, exposures were measured as the product of the dosing time and the increase in total chamber pressure for the dose. We followed a similar method of surface coverage to one reported previously.<sup>48–50</sup> However, the actual composition of the mixture may be different upon considering ionization sensitivity factors. The accepted sensitivity factor for water and ACN are 1.0 and 2.0, respectively.<sup>51</sup> For time-dependent as well as temperature-dependent studies, as prepared thin films were warmed at a rate of 5 K  $min^{-1}$  to the desired temperatures.

### 2.4 RAIRS setup

RAIR spectra were collected in the 4000–550  $cm^{-1}$  range with a spectral resolution of 2  $cm^{-1}$  using a Bruker Vertex 70 FT-IR spectrometer. The IR beam was taken out of the spectrometer using a gold-plated mirror and focused on the sample at an incident angle of  $80^\circ \pm 7^\circ$  through a ZnSe viewport. The reflected IR beam from the sample was re-focused using another gold-plated mirror to a liquid  $N_2$  cooled mercury cadmium telluride (MCT) detector. The IR beam outside of the vacuum chamber was purged with dry  $N_2$  to avoid background noise. To ensure better signal-to-noise ratio, each RAIR spectrum was averaged over 512 scans.

## 3 Results and discussion

We performed our study starting with the desorption behavior of ACN from 1:1 ice mixtures of ACN: $H_2O$  in the range of 125–

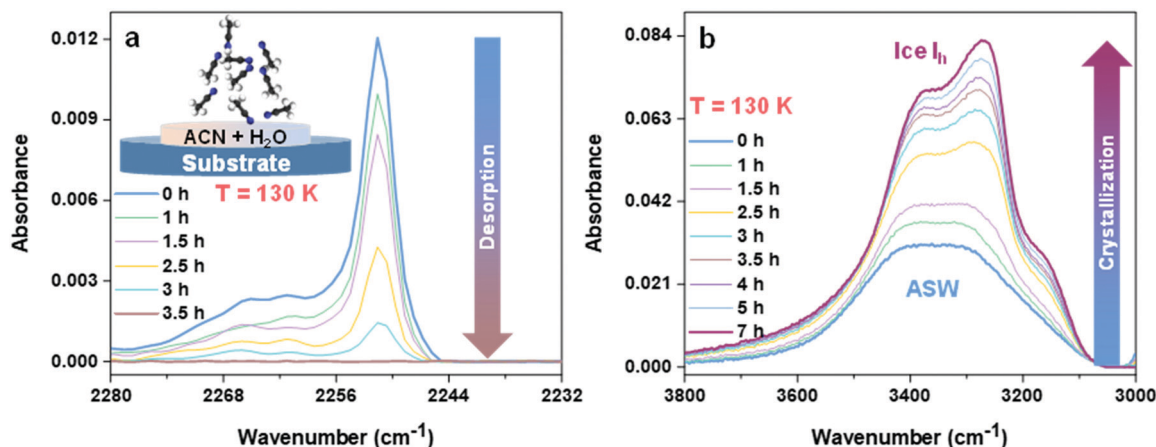


Fig. 1 Desorption induced ice crystallization. Isothermal time-dependent RAIR spectra of 300 MLs of 1:1 ACN:H<sub>2</sub>O at 130 K in the (a) C≡N stretching region and (b) O–H stretching region. The film was co-deposited on Ru(0001) at 10 K and then heated at a rate of 5 K min<sup>−1</sup> to 130 K. The C≡N stretching band at 2251 cm<sup>−1</sup> vanished due to desorption of ACN which transformed the broad O–H stretching band centered at ~3350 cm<sup>−1</sup> into ice I<sub>h</sub>. The inset in (a) shows the desorption of ACN from an ice mixture at 130 K.

135 K. As mentioned in the experimental section, the ratios are in terms of molar concentrations, assuming the same sticking coefficient for both the species. Fig. 1 shows the time-dependent RAIR spectra of 300 MLs of 1:1 ACN:H<sub>2</sub>O at 130 K. For this, mixed ice was co-deposited on Ru(0001) at 10 K and warmed to 130 K. The ice mixture was held at 130 K under vacuum for 7 h. Fig. 1a and b show time-dependent RAIR spectra at 130 K in the C≡N and O–H stretching regions, respectively. We will mainly focus on the C≡N stretch (2232–2280 cm<sup>−1</sup>) and O–H stretch (3000–3800 cm<sup>−1</sup>) where major changes were observed for the ACN:H<sub>2</sub>O films. The spectra of 150 MLs of pure ACN and of 300 MLs of ACN:H<sub>2</sub>O films with different ratios (1:1, 1:5, and 5:1) at 10 K are shown in Fig. S1A (ESI<sup>†</sup>) and the peak assignments for these are consistent with previous reports.<sup>52,53</sup> In Fig. 1a, at 0 h, corresponding to the first spectrum when the temperature equilibrates at 130 K, the C≡N stretching band shows a peak at 2251 cm<sup>−1</sup> which is the characteristic peak of pure ACN at 130 K. This peak is due to the phase separation of ACN from the H<sub>2</sub>O matrix as shown in Fig. S2b (ESI<sup>†</sup>), where the broad peak (2264 cm<sup>−1</sup>, attributed to hydrogen-bonded ACN with H<sub>2</sub>O)<sup>44,54</sup> at 10 K was reduced in intensity and shifted to 2251 cm<sup>−1</sup> (attributed to pure ACN) at 130–135 K, as reported in our previous study.<sup>44</sup> This was further confirmed by comparing the RAIR spectra of 150 MLs of pure ACN (Fig. S3, ESI<sup>†</sup>) with the spectra in Fig. 1a. The 2251 cm<sup>−1</sup> peak disappeared within 3.5 h due to the desorption of ACN from the ice mixture and is comparable to the desorption of 150 MLs of pure ACN within 3 h from the substrate, as shown in Fig. S3b (ESI<sup>†</sup>). The desorption behavior of ACN can be seen in the TPD mass spectra shown in Fig. S1B (ESI<sup>†</sup>), for different mixtures.

In Fig. 1b, the O–H stretching band showed a major change due to the desorption of ACN with time, at 130 K. At 0 h, the broad peak centered at ~3350 cm<sup>−1</sup> (after the phase separation of ACN from the ice mixture), is a distinctive feature of ASW. At 130 K, ACN desorbed gradually from the ice matrix and the

broad peak centered at ~3350 cm<sup>−1</sup> was red-shifted, manifesting an increase in order and number of H-bonded H<sub>2</sub>O molecules.<sup>55</sup> The peak gradually became sharp and was split within 7 h. Sharpening and splitting of the O–H stretching band were attributed to the crystallization of the ice film. The band splits, giving three peaks positioned at 3375, 3275, and 3165 cm<sup>−1</sup>, were assigned to ice I<sub>h</sub>. These assignments were confirmed by comparing the O–H stretching band of the ice film left after desorption of ACN at 130 K and of pure crystalline ice I<sub>h</sub>, as shown in Fig. S4a (ESI<sup>†</sup>). Both the bands are equivalent, which confirmed the formation of ice I<sub>h</sub> after desorption of ACN at 130 K. However, as shown in Fig. S4a (ESI<sup>†</sup>), the high-frequency shoulder at ~3380 cm<sup>−1</sup> increases in amplitude slightly for pure crystalline ice I<sub>h</sub> (red trace) compared to ice I<sub>h</sub> obtained from mixed ice (black trace) and this rise is attributed to the presence of grain-boundary water in the former case.<sup>56</sup> Furthermore, to confirm that ice crystallization is a desorption assisted process, we carried out two experiments. First, we performed an isothermal time-dependent RAIR study of 300 MLs of ACN:H<sub>2</sub>O in a 1:1 ratio at 120 K as shown in Fig. S8 (ESI<sup>†</sup>). Desorption of ACN (shown in Fig. S8b, ESI<sup>†</sup>) was not complete even after 51 h as the peak at 2251 cm<sup>−1</sup> did not vanish completely. In turn, the broad peak at ~3350 cm<sup>−1</sup> of the O–H stretching band shown in Fig. S8a (ESI<sup>†</sup>) remained broad, suggesting no crystallization. Also, we performed an isothermal time-dependent RAIR experiment of 150 MLs of solid H<sub>2</sub>O film at 130 K, as shown in Fig. S9 (ESI<sup>†</sup>). Self-crystallization of a solid H<sub>2</sub>O film was not observed even after 19 h. This proved that desorption of ACN from an ice mixture assists in crystallization of ice at a lower temperature than its normal crystallization temperature of 155 K.

Ice I<sub>h</sub> was formed *via* ACN desorption from 1:1 ACN:H<sub>2</sub>O films even at 125, 127, and 135 K as shown in Fig. S5–S7 (ESI<sup>†</sup>). We observed that with decreasing temperature, the time required for the desorption of ACN and crystallization of ice increased. Here, it was evident that desorption assisted ice I<sub>h</sub>

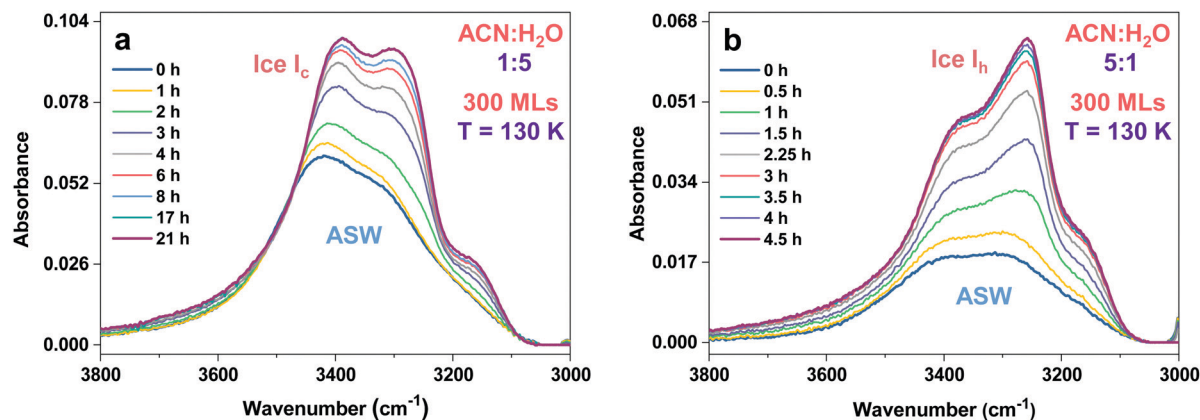


Fig. 2 (a) Time-dependent RAIR spectra of 300 MLs of 1:5 ACN:H<sub>2</sub>O film at 130 K in the O–H stretching region. The film was co-deposited on Ru(0001) at 10 K and then heated at a rate of 5 K min<sup>-1</sup> to 130 K. The first spectrum ( $t = 0$  h) is from a completely amorphous film and the last spectrum ( $t = 21$  h) is from a completely crystallized ice film. (b) Time-dependent RAIR spectra of 300 MLs of the 5:1 ACN:H<sub>2</sub>O film at 130 K in the O–H stretching region. The film was co-deposited on Ru(0001) at 10 K and then heated at a rate of 5 K min<sup>-1</sup> to 130 K. The first spectrum ( $t = 0$  h) is from a completely amorphous film and the last spectrum ( $t = 4.5$  h) is from a completely crystallized ice film.

crystallization follows certain kinetics. The crystallization kinetics of ice formation is of major importance for both terrestrial as well as extraterrestrial science. Isothermal time-dependent RAIR spectra of 1:1 ACN:H<sub>2</sub>O films at 125, 127, 130, and 135 K were used to evaluate the crystallization kinetics. These data are described in the Crystallization Kinetics section. Furthermore, the effect of the composition of the ice film on ice crystallization was also studied for ACN:H<sub>2</sub>O ratios of 1:5 and 5:1. The larger the fraction of ACN molecules in the ASW film, the faster the desorption of ACN and consequently the diffusion of H<sub>2</sub>O molecules. Fig. 2a shows the isothermal time-dependent RAIR spectra in the O–H stretching region of 300 MLs of 1:5 ACN:H<sub>2</sub>O film at 130 K. The associated desorption behavior of ACN from the ice film is shown in Fig. S10a (ESI<sup>†</sup>), where the C≡N stretching band consists of two types of peaks, attributed to hydrogen-bonded ACN (broad peak around 2266 cm<sup>-1</sup>)<sup>54</sup> and free ACN (peak at 2251 cm<sup>-1</sup>), respectively, at 130 K at 0 h. At 130 K, while the ACN phase separated for an ACN:H<sub>2</sub>O ratio of 1:1, the occurrence of a broad peak at 2266 cm<sup>-1</sup> for 1:5 ACN:H<sub>2</sub>O was surprising. Here, ACN could not phase-separate completely from the ice film even at 130 K because the number of ACN molecules was less and most of them were trapped in the ASW matrix. Several theoretical studies suggest<sup>57–59</sup> that ACN molecules can form a hydrate cluster (CH<sub>3</sub>CN)·(H<sub>2</sub>O)<sub>*n*</sub> ( $n > 1$ ) with varying number of H<sub>2</sub>O molecules which could also be a reason for ACN not being phase-separated at 130 K for the 1:5 ACN:H<sub>2</sub>O film. Because of the cluster formation between ACN and H<sub>2</sub>O, complete desorption of ACN from the ice film took a longer time of 4 h than the 1:1 ACN:H<sub>2</sub>O film. This restricted ACN desorption can also be seen in the TPD mass spectra shown in Fig. S1B (ESI<sup>†</sup>). The marked (with red star) desorption hump around 132 K along with the main desorption peak at ~140 K are attributed to the restricted ACN desorption from the 1:5 ACN:H<sub>2</sub>O film during annealing. On the other hand, the O–H stretching region showed (in Fig. 2a) a prominent

change with the restricted desorption of ACN from the film. The ASW feature at 0 h gradually became sharp and split into three peaks namely, 3395, 3290 and 3165 cm<sup>-1</sup>, with time. These features of the O–H stretching band correspond to ice I<sub>c</sub>, (Fig. S4b, ESI<sup>†</sup>) and are consistent with previous studies<sup>12,60,61</sup> including our earlier study<sup>12</sup> where we correlated the RAIRS and reflection high-energy electron diffraction (RHEED) data under similar experimental conditions. Limited (due to the smaller amount of ACN in the 1:5 ACN:H<sub>2</sub>O film) and obstructed (due to the cluster formation) desorption of ACN molecules from the ice film gave restricted mobility to the H<sub>2</sub>O molecules. In turn, ASW was restricted to metastable ice I<sub>c</sub> even after 21 h at 130 K. We performed similar isothermal time-dependent RAIR experiments for the 1:5 ACN:H<sub>2</sub>O film at 133 and 135 K and obtained similar results leading to ice I<sub>c</sub> as shown in Fig. S11, and S12, respectively (ESI<sup>†</sup>).

We performed another isothermal time-dependent experiment of 300 MLs with 5:1 ACN:H<sub>2</sub>O at 130 K. The O–H stretching region is shown in Fig. 2b and the associated ACN desorption behavior is shown in Fig. S10b (ESI<sup>†</sup>). At 0 h, the C≡N stretching band at 2251 cm<sup>-1</sup> (the same as obtained for the 1:1 ACN:H<sub>2</sub>O film) shown in Fig. S10b (ESI<sup>†</sup>) obtained after phase separation of ACN from the ice mixture at 130 K vanished within 3 h due to rapid desorption of the ACN molecules. The desorption of a large number of ACN molecules from the ice matrix provided a sufficiently high mobility to the H<sub>2</sub>O molecules. These mobile H<sub>2</sub>O molecules arranged most stably and resulted in ice I<sub>h</sub> within 4.5 h. It is evident that the ice I<sub>h</sub> formation from the 5:1 ACN:H<sub>2</sub>O film was faster than that of the 1:1 ACN:H<sub>2</sub>O film as expected due to bulk desorption of ACN in the former case. We obtained a similar result for the 5:1 ACN:H<sub>2</sub>O films at 133 and 135 K, shown in Fig. S13 and S14 (ESI<sup>†</sup>). Thus, we can form ice I<sub>c</sub> and ice I<sub>h</sub> selectively depending on the ice film compositions.

Formation of crystalline ice requires a sufficiently high mobility of water molecules for diffusion and molecular

rearrangement.<sup>36</sup> When ACN and water are co-deposited at 10 K, it forms a well-mixed system. Upon warming above 100 K, ACN molecules were phase-separated from water-ice<sup>44</sup> but they remain in the ice matrix. We suggest that during phase separation, ACN being a larger molecule, will increase the mobility/diffusion of water molecules, which will be further increased by the subsequent desorption of ACN after keeping the mixture at a given temperature for several hours. This desorption of the ACN molecules is the trigger for the diffusion/mobility of water that leads to the accelerated crystallization. In the case of the 1:5 mixture, due to the phase separation of smaller quantities of ACN and their desorption, ASW crystallization is restricted to metastable ice I<sub>c</sub>.

The present study and earlier reports on methanol,<sup>16</sup> acetone<sup>12</sup> and formaldehyde<sup>23</sup> show that the kinetics of crystallization is affected by the specific additives that are incorporated in the ASW film and a specific reason has been given for each. There may be one or several effects that might be causing the lowering of the onset temperature of crystallinity; it could be the desorption temperature, size, chemical nature or morphology of the co-deposited molecules. In the present case, it is the desorption (temperature) of the co-adsorbed molecule, which is affecting the crystallization kinetics of ASW. It may require additional theoretical as well as experimental investigations to correlate the effect of different molecules on ASW crystallization.

### Crystallization kinetics

Time-dependent RAIR spectra of 1:1 ACN:H<sub>2</sub>O films were utilized to evaluate the crystallization of ASW under isothermal conditions at the corresponding temperatures (125, 127, 130, and 135 K, shown in Fig. 1b and Fig. S5–S7, ESI†). The volatile O–H stretching bands of RAIRS were utilized to estimate the crystallization kinetics of ASW crystallization in previous reports.<sup>12,17,23,62,63</sup> Here, we adopted a similar approach.

Fig. 3(a) shows the time-dependent RAIR spectra for 300 MLs of 1:1 ACN:H<sub>2</sub>O film kept at 127 K. The first spectrum (0 h trace) in Fig. 3a is from a completely amorphous film and

the last spectrum (21 h) is from a completely crystalline film. The intermediate spectra represent the progress of crystallization and are a combination of pure amorphous and pure crystalline spectra. The vertical dashed line at a fixed wavenumber (3268 cm<sup>-1</sup>) was used to evaluate the crystallization fraction for each temperature.

Fig. 3b shows the crystallization fraction *versus* time obtained from vertical cuts through the time series spectra of O–H stretching bands for a set of isothermal time-dependent experiments (shown in Fig. S5a, S6a and S7a, ESI†), analogous to those shown in Fig. 3a at different temperatures. The crystallization fraction,  $x(t)$  was calculated by eqn (1),

$$x(t) = \frac{\Delta A(1)}{\Delta A(2)} \quad (1)$$

where  $\Delta A(1)$  is the difference in the absorbance at a particular time  $t$  and that at time zero, and  $\Delta A(2)$  is the difference in absorbance of a completely crystallized film and that of a completely amorphous film.

In Fig. 3b the change of the shape of the curve from sigmoidal to an exponential, manifests an increase in crystallization kinetics with increasing temperature.<sup>12,17</sup> Various crystallization parameters for ASW were evaluated by fitting the crystallization fraction to the Avrami equation<sup>64,65</sup> at different temperatures. The Avrami equation is

$$x(t) = 1 - \exp(-k \cdot t^n) \quad (2)$$

where  $k$  is the rate constant,  $t$  is time, and  $n$  is an exponent. For all temperatures,  $n$  can hold close to integer values between 1 to 4 and this predicts the nature of the crystallization process. After arranging eqn (2) in linear form, the equation becomes

$$\ln(-\ln[1 - x(t)]) = n \ln(t) + n \ln k \quad (3)$$

Fig. 4a shows  $\ln(-\ln[1 - x(t)])$  *versus*  $\ln(t)$  plotted for different temperatures using eqn (3). The slope and intercept of linearly fitted lines were utilized to estimate the value of  $n$  and  $k$  for different temperatures. The obtained values of  $n$  and

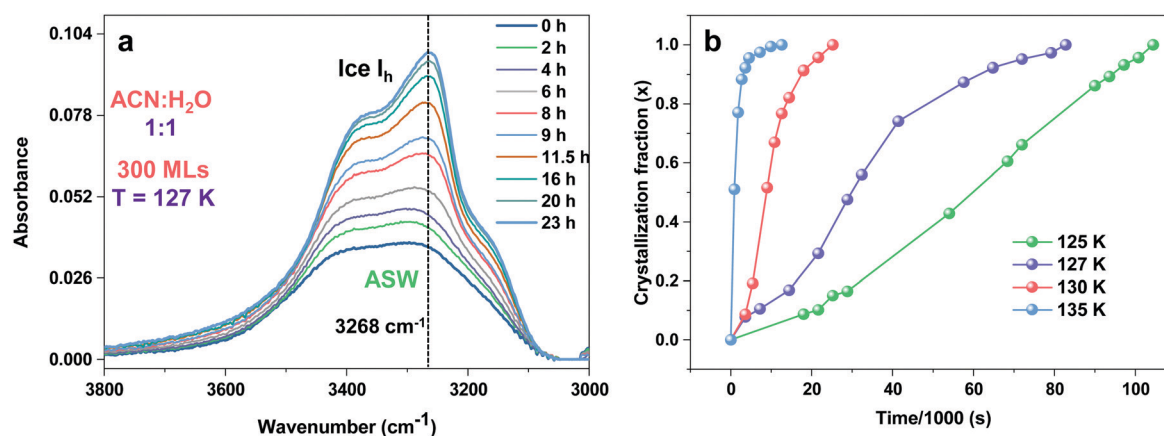


Fig. 3 (a) Time-dependent RAIR spectra of 300 MLs of the 1:1 ACN:H<sub>2</sub>O film at 127 K in the O–H stretching region. The film was co-deposited on Ru(0001) at 10 K and heated at a rate of 5 K min<sup>-1</sup> to 127 K. (b) Crystallization fraction *versus* time for 300 MLs of the 1:1 ACN:H<sub>2</sub>O film obtained from isothermal RAIR measurements at 125, 127, 130, and 135 K. The crystallization fraction was calculated from a vertical cut at 3268 cm<sup>-1</sup> in the O–H stretching band for a set of time-dependent RAIRS spectra shown in Fig. 1a and Fig. S5a, S6a, and S7a (ESI†).

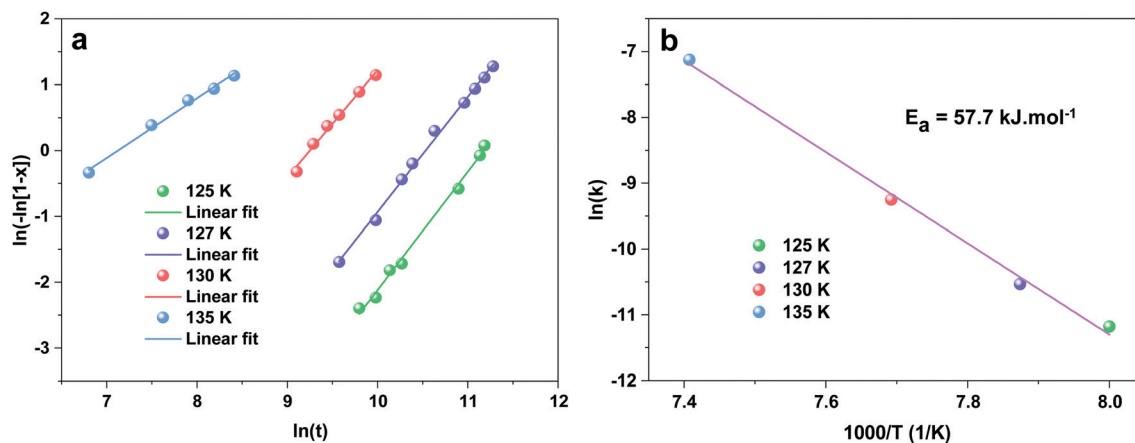


Fig. 4 A plot of the linearized form of the Avrami equation for ASW crystallization. Plots of  $\ln(-\ln[1-x])$  vs.  $\ln(t)$  at different temperatures of 125, 127, 130, and 135 K were made using the O–H stretching bands. The obtained data points were fitted using the Avrami equation. (b) Arrhenius plot of  $\ln k$  versus  $(1/T)$ , achieved from the analysis the slope and intercept of the linearly fitted lines of plot (a) for different temperatures. The activation energy ( $E_a$ ) of ice crystallization was calculated from the slope of the linearly fitted straight line of plot (b).

$k$  are listed in Table S1 (ESI<sup>†</sup>). The estimated value of  $k$  in this study is larger than the previously reported values estimated in similar experimental conditions,<sup>23,62</sup> which, further, presents evidence for accelerated crystallization.

The value obtained for  $n$  was between 1.80 to 0.90 for different temperatures. With the input of previous studies we note that for the evaluated value of  $n$ , crystallization kinetics is a diffusion-controlled phenomenon with particles growing into predominantly spherical geometry,<sup>12,23,62,63,66–68</sup> and it is evident that ACN desorption from an ice mixture provides enough mobility for water volatile molecules for rearrangement and crystallization. However, crystallization of ASW gives an  $n$  value equal to  $\sim 4$ , and suggests three-dimensional growth and random nucleation.<sup>62,69,70</sup> Our values of  $n$  are, however, lower and suggest low dimensional growth. This is reasonable because ACN is undergoing phase separation but within the ice-matrix in the form of small domains. These domains can be present at bulk and at interfaces in the ice-matrix. When the ACN molecules desorbed from such domains, they will induce (diffusion/mobility) crystallization and will prevent three-dimensional growth.<sup>12,23</sup> The activation energy ( $E_a$ ) of ice crystallization was estimated from the slope of the linearly fitted line of the Arrhenius plot (Fig. 4b,  $\ln k$  versus  $(1/T)$ ). The evaluated activation energy in this study was  $\sim 57.7 \text{ kJ mol}^{-1}$  and it is comparable with that of the previously reported value for the crystallization of pure ASW.<sup>17,62,69,71,72</sup> Here, early ice  $I_h$  crystallization from 1:1 ACN:H<sub>2</sub>O films can be attributed to the desorption assisted mobility of H<sub>2</sub>O molecules. Due to sufficient mobility, H<sub>2</sub>O molecules occupied the thermodynamically most stable sites and resulted in ice  $I_h$  at a lower temperature (125–135 K) than the usual ice  $I_h$  crystallization temperature.

## 4 Conclusions

We have established an isothermal route for the formation of either ice  $I_c$  and ice  $I_h$ , induced by the desorption of ACN from

ice mixtures depending upon their compositions at 130–135 K in an UHV. We were also able to form ice  $I_h$  at 125 K which is a much lower temperature than the usual crystallization temperature in UHV conditions. Associated crystallization kinetics for ice  $I_h$  and the activation energy of crystallization were evaluated by using isothermal time-dependent RAIR spectra at 125–135 K for a 1:1 ACN:H<sub>2</sub>O film. We assumed that the extent of desorption of ACN and relative (simultaneous) diffusion of H<sub>2</sub>O molecules played an important role in ice crystallization at low temperatures. Such studies will be of importance in astrophysical environments or ISM.

## Author contributions

T. P. proposed the project and supervised the progress. G. V. designed and performed the experiments. G. V and J. G. analyzed the results. The manuscript was written through contributions of all the authors.

## Conflicts of interest

The authors declare no competing financial interests.

## Acknowledgements

We acknowledge the Science and Engineering Research Board (SERB), Department of Science and Technology (DST), Government of India for research funding. We thank Dr Bhalamurugan Sivaraman and Dr Rabin Rajan J. Methikkalam for helpful comments and discussions. We also thank Mr Bijesh Malla, Mr Chandan Bhat, Mr Pillalamarri Srikrishnarka, and Dr Tripti Ahuja for their valuable input in relation to this work. G. V. thanks IITM for his research fellowship. J. G. acknowledges IIT Madras for an institute postdoctoral fellowship.

## References

- 1 A. C. Cheung, D. M. Rank, C. H. Townes, D. D. Thornton and W. J. Welch, Detection of water in interstellar regions by its microwave radiation, *Nature*, 1969, **221**, 626–628.
- 2 E. L. Gibb, D. C. B. Whittet, A. C. A. Boogert and A. G. G. M. Tielens, Interstellar Ice: The Infrared Space Observatory Legacy, *Astrophys. J., Suppl. Ser.*, 2004, **151**, 35–73.
- 3 W. J. Gillett and F. C. Forrest, Spectra of the Becklin-Neugebauer point source and the Kleinmann-Low nebula from 2.8 to 13.5 microns, *Astrophys. J.*, 1973, **179**, 483–491.
- 4 T. Bartels-Rausch, V. Bergeron, J. H. E. Cartwright, R. Escribano, J. L. Finney, H. Grothe, P. J. Gutiérrez, J. Haapala, W. F. Kuhs, J. B. C. Pettersson, S. D. Price, I. Sainz-Díaz, D. J. Stokes, G. Strazzulla, E. S. Thomson, H. Trinks and N. Uras-Aytemiz, Ice structures, patterns, and processes: A view across the ice fields, *Rev. Mod. Phys.*, 2012, **84**, 885.
- 5 C. A. Angell, Amorphous Water, *Annu. Rev. Phys. Chem.*, 2004, **55**, 559–583.
- 6 T. Loerting, K. Winkel, M. Seidl, M. Bauer, C. Mitterdorfer, P. H. Handle, C. G. Salzmänn, E. Mayer, J. L. Finney and D. T. Bowron, How many amorphous ices are there?, *Phys. Chem. Chem. Phys.*, 2011, **13**, 8783–8794.
- 7 C. G. Salzmänn, P. G. Radaelli, B. Slater and J. L. Finney, The polymorphism of ice: Five unresolved questions, *Phys. Chem. Chem. Phys.*, 2011, **13**, 18468–18480.
- 8 N. Watanabe and A. Kouchi, Ice surface reactions: A key to chemical evolution in space, *Prog. Surf. Sci.*, 2008, **83**, 439–489.
- 9 W. F. Kuhs, C. Sippel, A. Falenty and T. C. Hansen, Extent and relevance of stacking disorder in ‘ice Ic’, *Proc. Natl. Acad. Sci. U. S. A.*, 2012, **109**, 21259–21264.
- 10 T. L. Malkin, B. J. Murray, C. G. Salzmänn, V. Molinero, S. J. Pickering and T. F. Whale, Stacking disorder in ice I, *Phys. Chem. Chem. Phys.*, 2014, **17**, 60–76.
- 11 J. Ghosh, R. R. J. Methikkalam, R. G. Bhuin, G. Ragupathy, N. Choudhary, R. Kumar and T. Pradeep, Clathrate hydrates in interstellar environment, *Proc. Natl. Acad. Sci. U. S. A.*, 2019, **116**, 1526–1531.
- 12 J. Ghosh, R. G. Bhuin, G. Vishwakarma and T. Pradeep, Formation of Cubic Ice via Clathrate Hydrate, Prepared in Ultrahigh Vacuum under Cryogenic Conditions, *J. Phys. Chem. Lett.*, 2020, **11**, 26–32.
- 13 J. Ghosh, R. G. Bhuin, G. Ragupathy and T. Pradeep, Spontaneous Formation of Tetrahydrofuran Hydrate in Ultrahigh Vacuum, *J. Phys. Chem. C*, 2019, **123**, 16300–16307.
- 14 J. Ghosh, Propane and propane – water interactions: a study at cryogenic temperatures †, *Phys. Chem. Chem. Phys.*, 2018, **20**, 1838–1847.
- 15 R. G. Bhuin, R. R. J. Methikkalam, S. Bag and T. Pradeep, Diffusion and Crystallization of Dichloromethane within the Pores of Amorphous Solid Water, *J. Phys. Chem. C*, 2016, **120**, 13474–13484.
- 16 R. Souda, Effects of methanol on crystallization of water in the deeply supercooled region, *Phys. Rev. B: Condens. Matter Mater. Phys.*, 2007, **75**, 184116.
- 17 D. H. Lee and H. Kang, Acid-Promoted Crystallization of Amorphous Solid Water, *J. Phys. Chem. C*, 2018, **122**, 24164–24170.
- 18 S. M. McClure, E. T. Barlow, M. C. Akin, P. L. Tanaka, D. J. Safarik, T. M. Truskett and C. B. Mullins, Effect of dilute nitric acid on crystallization and fracture of amorphous solid water films, *J. Phys. Chem. C*, 2007, **111**, 10438–10447.
- 19 A. Falenty, T. C. Hansen and W. F. Kuhs, Cubic Ice Formation and Annealing during CO<sub>2</sub> Clathrate Hydrate Decomposition at Low Temperatures, *Phys. Chem. Ice*, 2010, 411.
- 20 A. Falenty and W. F. Kuhs, ‘Self-Preservation’ of CO<sub>2</sub> Gas Hydrates-Surface Microstructure and Ice Perfection, *J. Phys. Chem. B*, 2009, **113**, 15975–15988.
- 21 W. F. Kuhs, G. Genov, D. K. Staykova and T. Hansen, Ice perfection and onset of anomalous preservation of gas hydrates, *Phys. Chem. Chem. Phys.*, 2004, **6**, 4917–4920.
- 22 S. Takeya, T. Uchida, J. Nagao, R. Ohmura, W. Shimada, Y. Kamata, T. Ebinuma and H. Narita, Particle size effect of CH<sub>4</sub> hydrate for self-preservation, *Chem. Eng. Sci.*, 2005, **60**, 1383–1387.
- 23 J. Ghosh, G. Vishwakarma, S. Das and T. Pradeep, Facile Crystallization of Ice Ih via Formaldehyde Hydrate in Ultrahigh Vacuum under Cryogenic Conditions, *J. Phys. Chem. C*, 2021, **125**, 4532–4539.
- 24 L. G. Dowell and A. P. Rinfret, Low-temperature forms of ice as studied by X-ray diffraction, *Nature*, 1960, **188**, 1144–1148.
- 25 J. A. McMillan and S. C. Los, Vitreous ice: Irreversible transformations during warm-up, *Nature*, 1965, **206**, 806–807.
- 26 E. Mayer and A. Hallbrucker, Cubic ice from liquid water, *Nature*, 1987, **325**, 601–602.
- 27 T. L. Malkin, B. J. Murray, A. V. Brukhno, J. Anwar and C. G. Salzmänn, Structure of ice crystallized from supercooled water, *Proc. Natl. Acad. Sci. U. S. A.*, 2012, **109**, 1041–1045.
- 28 B. J. Murray, D. A. Knopf and A. K. Bertram, The formation of cubic ice under conditions relevant to Earth’s atmosphere, *Nature*, 2005, **434**, 202–205.
- 29 B. J. Murray and A. K. Bertram, Formation and stability of cubic ice in water droplets, *Phys. Chem. Chem. Phys.*, 2006, **8**, 186–192.
- 30 Y. P. Handa, D. D. Klug and E. Whalley, Energies of the phases of ice at low temperature and pressure relative to ice Ih, *Can. J. Chem.*, 1988, **66**, 919–924.
- 31 J. E. Bertie, L. D. Calvert and E. Whalley, Transformations of ice II, Ice III, and ice v at atmospheric pressure, *J. Chem. Phys.*, 1963, **38**, 840–846.
- 32 V. Petrenko and R. Whitworth, *Physics of ice*, Oxford, 2002.
- 33 J. C. Dore, M. Dunn and P. Chieux, Neutron diffraction studies of ice nucleation in porous silica, *J. Phys., Colloq.*, 1987, **48**, 457–463.
- 34 D. C. Steytler, J. C. Dore and C. J. Wright, Neutron diffraction study of cubic ice nucleation in a porous silica network, *J. Phys. Chem.*, 1983, **87**, 2458–2459.

- 35 J. M. Baker, J. C. Dore and P. Behrens, Nucleation of ice in confined geometry, *J. Phys. Chem. B*, 1997, **101**, 6226–6229.
- 36 T. Hama, S. Ishizuka, T. Yamazaki, Y. Kimura, A. Kouchi, N. Watanabe, T. Sugimoto and V. Pirronello, Fast crystalline ice formation at extremely low temperature through water/neon matrix sublimation, *Phys. Chem. Chem. Phys.*, 2017, **19**, 17677–17684.
- 37 P. M. Solomon, K. B. Jefferts, A. A. Penzias and R. W. Wilson, Detection of Millimeter Emission Lines from Interstellar Methyl Cyanide, *Astrophys. J.*, 1971, **168**, L107.
- 38 B. L. Ulich and E. K. Conklin, Detection of methyl cyanide in Comet Kohoutek, *Nature*, 1974, **248**, 121.
- 39 A. J. McKay, M. A. DiSanti, M. S. P. Kelley, M. M. Knight, M. Womack, K. Wierzchos, O. H. Pinto, B. Bonev, G. L. Villanueva, N. Dello Russo, A. L. Cochran, N. Biver, J. Bauer, R. J. Vervack, E. Gibb, N. Roth and H. Kawakita, The peculiar volatile composition of co-dominated comet C/2016 R2 (PanSTARRS), *Astron. J.*, 2019, **158**, 128.
- 40 M. A. Cordiner, S. N. Milam, N. Biver, D. Bockelée-Morvan, N. X. Roth, E. A. Bergin, E. Jehin, A. J. Remijan, S. B. Charnley, M. J. Mumma, J. Boissier, J. Crovisier, L. Paganini, Y. J. Kuan and D. C. Lis, Unusually high CO abundance of the first active interstellar comet, *Nat. Astron.*, 2020, **4**, 861–866.
- 41 D. Bodewits, J. W. Noonan, P. D. Feldman, M. T. Bannister, D. Farnocchia, W. M. Harris, J. Y. Li, K. E. Mandt, J. W. Parker and Z. X. Xing, The carbon monoxide-rich interstellar comet 2I/Borisov, *Nat. Astron.*, 2020, **4**, 867–871.
- 42 J. Klinger, Extraterrestrial Ice. A Review, *J. Phys. Chem.*, 1983, **87**, 4209–4214.
- 43 S. Bag, R. G. Bhui, R. R. J. Methikkalam, T. Pradeep, L. Kephart, J. Walker, K. Kuchta, D. Martin and J. Wei, Development of ultralow energy (1–10 eV) ion scattering spectrometry coupled with reflection absorption infrared spectroscopy and temperature programmed desorption for the investigation of molecular solids, *Rev. Sci. Instrum.*, 2014, **85**, 1–7.
- 44 R. G. Bhui, R. R. J. Methikkalam, B. Sivaraman and T. Pradeep, Interaction of Acetonitrile with Water-Ice: An Infrared Spectroscopic Study, *J. Phys. Chem. C*, 2015, **119**, 11524–11532.
- 45 R. G. Bhui, R. R. J. Methikkalam, S. Bag and T. Pradeep, Diffusion and Crystallization of Dichloromethane within the Pores of Amorphous Solid Water, *J. Phys. Chem. C*, 2016, **120**, 13474–13484.
- 46 R. R. J. Methikkalam, R. G. Bhui, J. Ghosh, B. Sivaraman and T. Pradeep, Interaction of Acetonitrile with Alcohols at Cryogenic Temperatures, *J. Phys. Chem. C*, 2017, **121**, 2822–2835.
- 47 R. Rajan, J. Methikkalam, J. Ghosh, R. Gobinda Bhui, S. Bag, G. Ragupathy and T. Pradeep, Iron assisted formation of CO<sub>2</sub> over condensed CO and its relevance to interstellar chemistry †, *Phys. Chem. Chem. Phys.*, 2020, **22**, 8491.
- 48 H. Kang, T. H. Shin, S. C. Park, I. K. Kim and S. J. Han, Acidity of hydrogen chloride on ice, *J. Am. Chem. Soc.*, 2000, **122**, 9842–9843.
- 49 Y. Kim, E. S. Moon, S. Shin and H. Kang, Acidic water monolayer on ruthenium(0001), *Angew. Chem., Int. Ed.*, 2012, **51**, 12806–12809.
- 50 J. E. Schaff and J. T. Roberts, Toward an understanding of the surface chemical properties of ice: Differences between the amorphous and crystalline surfaces, *J. Phys. Chem.*, 1996, **100**, 14151–14160.
- 51 J. E. Bartmess and R. M. Georgiadis, Empirical methods for determination of ionization gauge relative sensitivities for different gases, *Vacuum*, 1983, **33**, 149–153.
- 52 E. L. Pace and L. J. Noe, Infrared Spectra of Acetonitrile and Acetonitrile-d<sub>3</sub>, *J. Chem. Phys.*, 1968, **49**, 5317–5325.
- 53 M. P. Marzocchi and S. Dobos, Infrared spectra and crystal structure of CH<sub>3</sub>CN and CD<sub>3</sub>CN. Polarization and intensity measurements, *Spectrochim. Acta, Part A*, 1974, **30**, 1437–1444.
- 54 J. E. Schaff and J. T. Roberts, Interaction of Acetonitrile with the Surfaces of Amorphous and Crystalline Ice, *Langmuir*, 1999, **15**, 7232–7237.
- 55 E. H. G. Backus, M. L. Grecea, A. W. Kleyn and M. Bonn, Surface crystallization of amorphous solid water, *Phys. Rev. Lett.*, 2004, **92**, 236101.
- 56 T. Kondo, H. S. Kato, M. Kawai and M. Bonn, The distinct vibrational signature of grain-boundary water in nanocrystalline ice films, *Chem. Phys. Lett.*, 2007, **448**, 121–126.
- 57 A. Chaudhari and S. L. Lee, Density Functional study of hydrogen-bonded acetonitrile-water complex, *Int. J. Quantum Chem.*, 2005, **102**, 106–111.
- 58 D.-S. Ahn and S. Lee, Computational Study of  $\sigma$ - and  $\pi$ -type Hydrogen Bonding in Acetonitrile-Water Clusters, *Bull. Korean Chem. Soc.*, 2003, **24**, 545.
- 59 R. Gopi, N. Ramanathan and K. Sundararajan, Acetonitrile-water hydrogen-bonded interaction: Matrix-isolation infrared and ab initio computation, *J. Mol. Struct.*, 2015, **1094**, 118–129.
- 60 W. Hagen, A. G. G. M. Tielens and J. M. Greenberg, The infrared spectra of amorphous solid water and ice Ic between 10 and 140 K, *Chem. Phys.*, 1981, **56**, 367–379.
- 61 E. Whalley, A detailed assignment of the O–H stretching bands of ice I, *Can. J. Chem.*, 1977, **55**, 3429–3441.
- 62 R. S. Smith, J. Matthiesen, J. Knox and B. D. Kay, Crystallization kinetics and excess free energy of H<sub>2</sub>O and D<sub>2</sub>O nanoscale films of amorphous solid water, *J. Phys. Chem. A*, 2011, **115**, 5908–5917.
- 63 R. S. Smith, N. G. Petrik, G. A. Kimmel and B. D. Kay, Thermal and nonthermal physiochemical processes in nanoscale films of amorphous solid water, *Acc. Chem. Res.*, 2012, **45**, 33–42.
- 64 M. Avrami, Kinetics of phase change. I: General theory, *J. Chem. Phys.*, 1939, **7**, 1103–1112.
- 65 M. Avrami, Kinetics of phase change. II Transformation-time relations for random distribution of nuclei, *J. Chem. Phys.*, 1940, **8**, 212–224.
- 66 W. Hage, A. Hallbrucker, E. Mayer and G. P. Johari, Crystallization kinetics of water below 150 K, *J. Chem. Phys.*, 1994, **100**, 2743–2747.
- 67 R. H. Doremus, *Rates of phase transformations*, Academic Press, New York, 1985.

- 68 C. N. R. Rao and K. J. Rao, *Phase transitions in solids: an approach to the study of the chemistry and physics of solids*, McGraw-Hill, New York, 1978.
- 69 T. Kondo, H. S. Kato, M. Bonn and M. Kawai, Deposition and crystallization studies of thin amorphous solid water films on Ru(0001) and on CO-precovered Ru(0001), *J. Chem. Phys.*, 2007, **127**, 094703.
- 70 Z. Dohnálek, G. A. Kimmel, R. L. Ciolli, K. P. Stevenson, R. S. Smith and B. D. Kay, The effect of the underlying substrate on the crystallization kinetics of dense amorphous solid water films, *J. Chem. Phys.*, 2000, **112**, 5932–5941.
- 71 D. J. Safarik and C. B. Mullins, The nucleation rate of crystalline ice in amorphous solid water, *J. Chem. Phys.*, 2004, **121**, 6003–6010.
- 72 C. Yuan, R. S. Smith and B. D. Kay, Communication: Distinguishing between bulk and interface-enhanced crystallization in nanoscale films of amorphous solid water, *J. Chem. Phys.*, 2017, **146**, 031102.